SUPPORTING INFORMATION

Effect of anisotropy of cellulose nanocrystal suspensions on stratification, domain structure formation and structural color

Konrad W. Klockars[1], Blaise L. Tardy[1,], Maryam Borghei[1], Anurodh Tripathi[1,2], Luiz G. Greca[1], Orlando J. Rojas[1,2,3,*]*

[1]Department of Bioproducts and Biosystems, School of Chemical Engineering, Aalto University, FI-00076 Aalto, Finland

[2]Department of Chemical and Biomolecular Engineering, North Carolina State University, Raleigh, NC 27695, USA

[3]Department of Applied Physics, School of Science, Aalto University, FI-00076 Aalto, Finland.

This supporting information document contains seven (7) Figures for a total of nine (9) pages.

Discussion S1: Characterization of the cellulose nanocrystal raw material

The pH, zeta potential and hydrodynamic radius (as obtained by dynamic light scattering and assuming a spherical form) for the CNCs used in this study correspond to 6.6, -32,7 ± 11 mV and 68.5 nm, respectively. The pH value is higher than for conventional CNC suspensions produced by sulfuric acid hydrolysis of cotton at the laboratory scale, having proton counter ions on the sulfate half-ester groups, or other reports that have used commercially-obtained CNCs.[1] The results indicate the sodium form of the CNCs, as previously reported for such nanoparticles.[2] The zeta potential is slightly lower than those measured by others for the same source.[2-5] The particle size measurement by DLS (hydrodynamic radius R_H) yields an average size of ~69 nm, reminiscent of previous values obtained for the same CNCs.[3] Importantly, the correlation data obtained by light scattering suggest a good dispersion and the absence of aggregates as judged by the sharp transition from high correlation to low correlation values and the unimodal curve (**Figure S1**). Surface charge measurements of the same commercial CNCs have been conducted in previous work by Reid et al.[3] (340 mmol/g) and Zoppe et al.[6] (208 mmol/g). In this study, no aggregation or change of opacity could be observed by the naked eye or in photographic images of the suspensions, even after several months, for all suspensions.

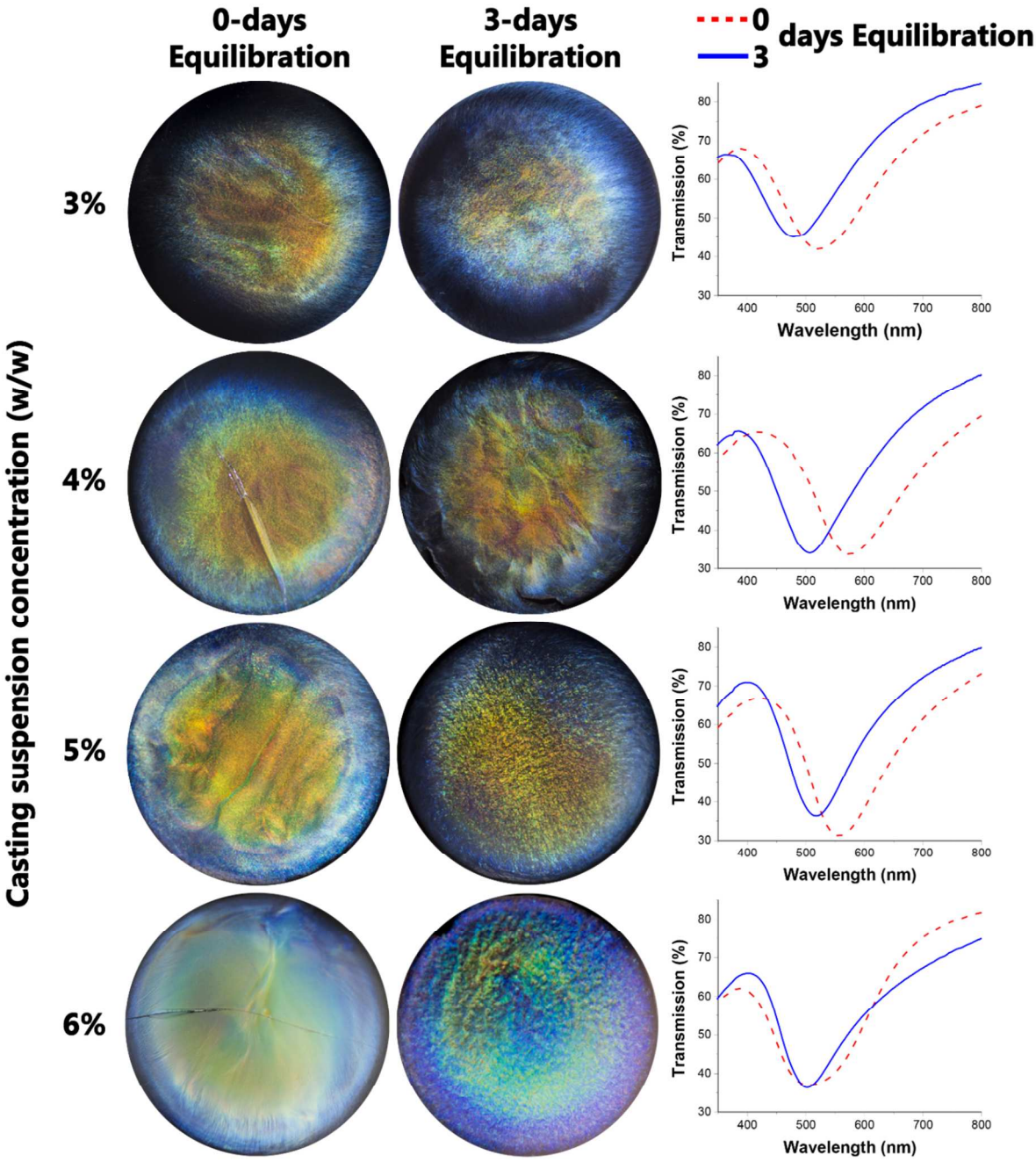

Figure S1. The films shown here belong to a sample set identical to the set N3, N4, N5, N6, E3, E4, E5, E6, except for the following changes: The films were cast on treated substrates washed with ethanol, instead of water, and the equilibration times were 0 and 3 days, instead of 0 and 7. The film photographs were taken with a Nikon D7200 camera, against a black background. The camera and light source were facing the films at an angle approximately perpendicular to the film surface. UV-Vis transmission spectra of the films in the corresponding row, showing the difference between equilibration and lack of equilibration at each casting concentration.

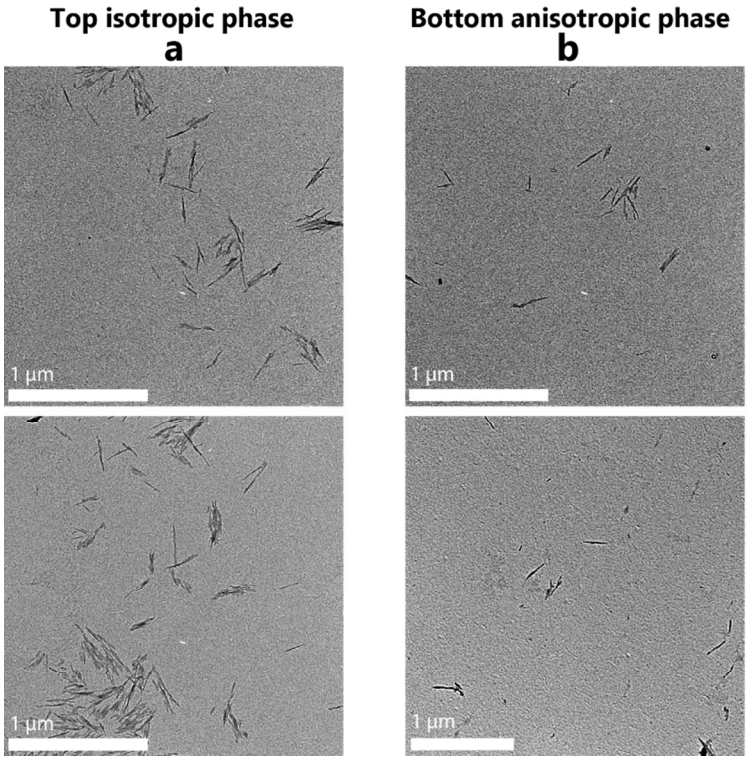

c

Model	GaussAmp
Equation	y=y0+A*exp(-0.5*((x-xc)/w)^2)
Plot	Counts
y0	0.54591 ± 0.86253
xc	121.39723 ± 1.73332
w	33.6483 ± 2.42039
A	22.44692 ± 1.19684
Reduced Chi-Sqr	1.984854621
R-Square (COD)	0.980510864
Adj. R-Square	0.972158377

Figure S2. TEM images used for determining the size distributions (**Figure 6 b_2, c_2**) of the (a) isotropic volume fraction, and (b) anisotropic volume fraction. (c) Parameters used in the Gaussian fit in **Figure 6 b_2**. The particles are more scarcely distributed in the images in (b), potentially because of excess blotting (see section 2.4).

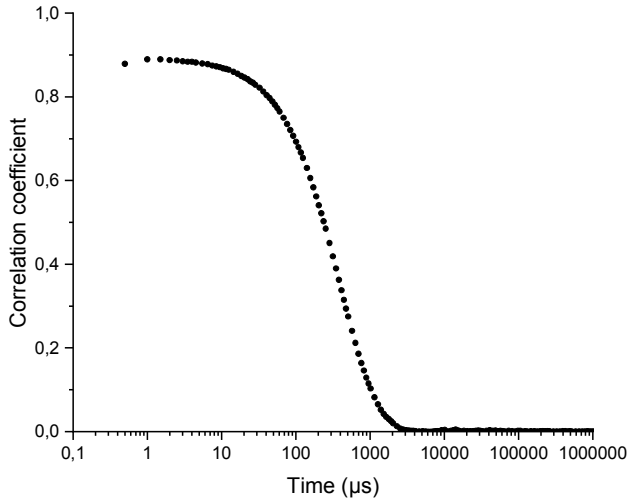

Figure S3. The raw correlation data from dynamic light scattering measurements. The unimodal correlogram, with a sharp transition between high and low correlation coefficients is indicative of a well dispersed suspension without clusters.

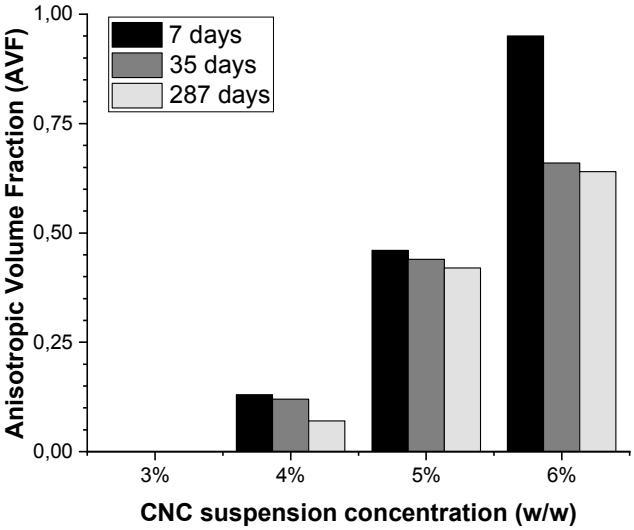

Figure S4. The anisotropic volume fraction of CNC suspensions as a function of concentration, measured after different time lapses after the suspension was prepared and left to equilibrate.

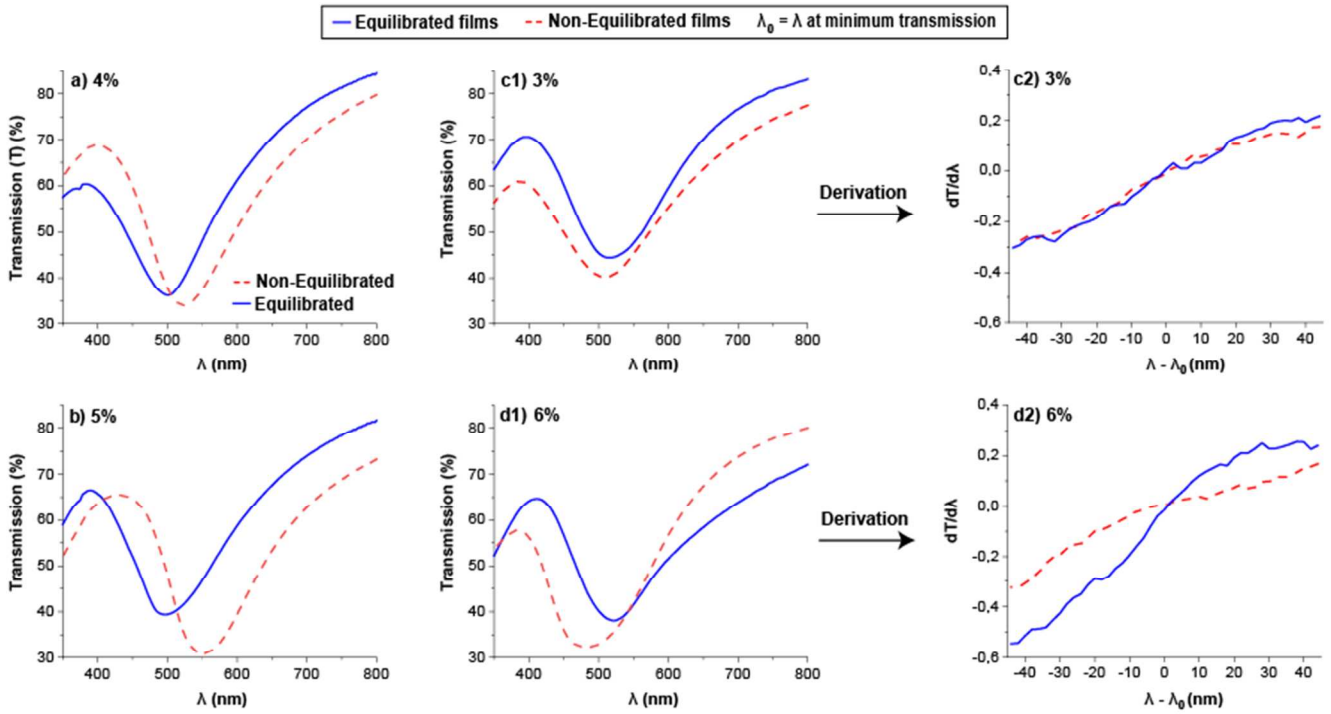

Figure S5. UV-vis transmission data collected from the (a) E4/N4, (b) E5/N5, (c_1) E3/N3 and (d_1) E6/N6 sample films. The blue profiles correspond to the equilibrated and the dotted red lines correspond to the non-equilibrated samples. The spectra in (a, b, c_1, d_1) are averages of three measurement points. (c_2) and (d_2) are derivatives of the spectra in (c_1) and (d_1), where the 0 wavelength corresponds to the minimum transmission value of the spectra. Steeper derivative profiles indicate narrower transmission spectral bandwidths, hinting to the presence of narrower pitch size distributions.

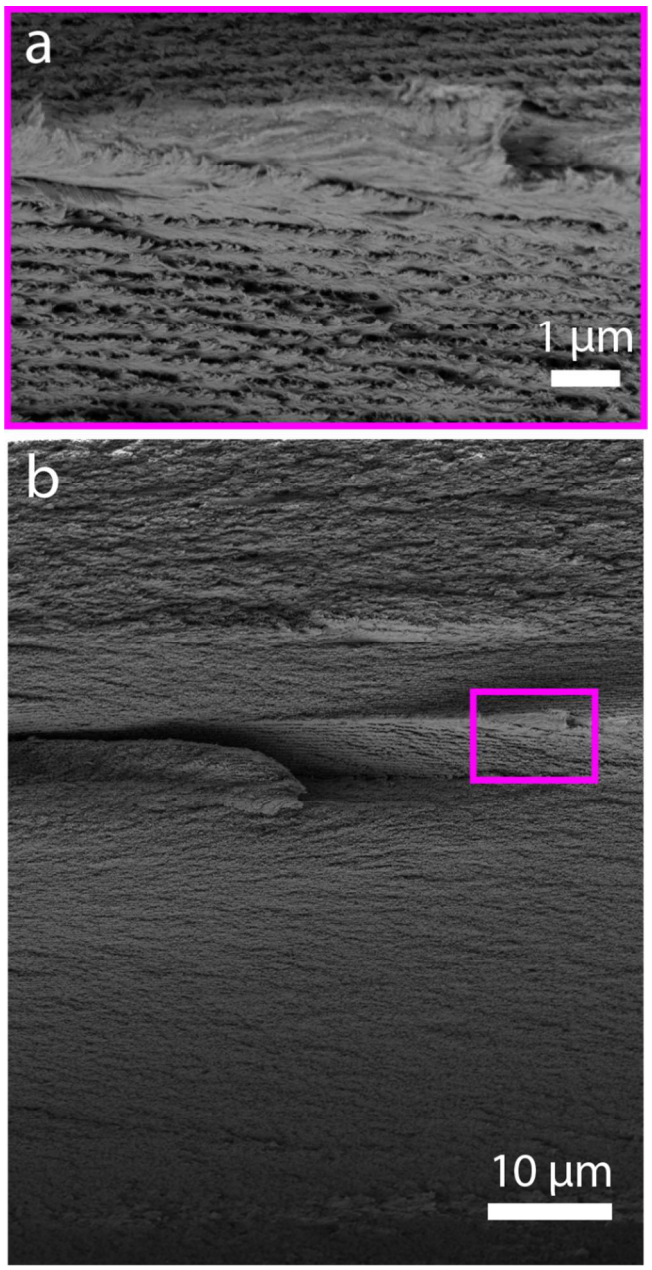

Figure S6. An ellipsoidal domain protruding from the middle layer of the E6 fractured film, viewed in its cross-section. (a) Higher magnification image of the purple rectangle in (b). (a) is identical to Figure $4a_5$.

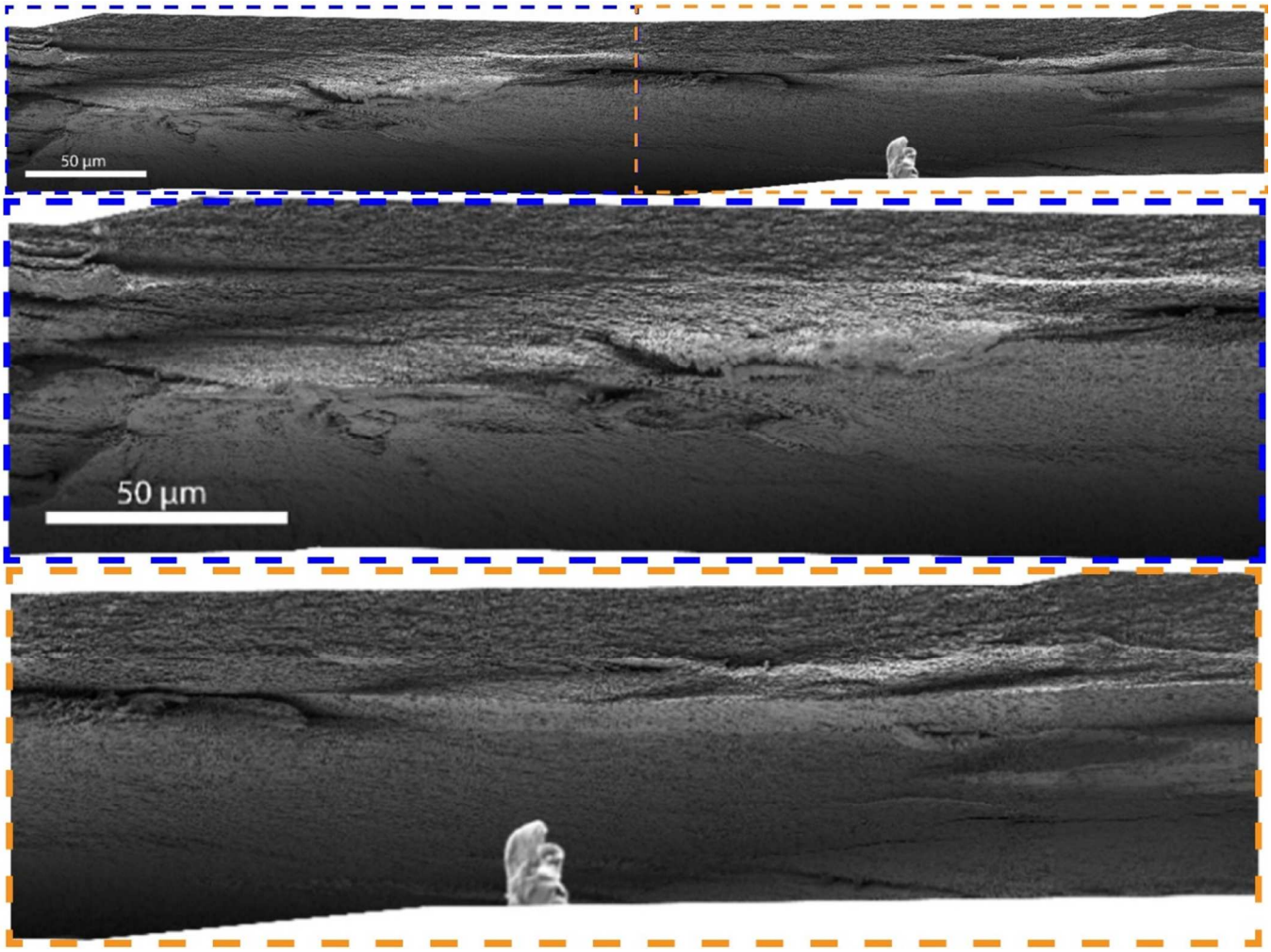

Figure S7. A sequence of 12 individual SEM images corresponding to the E6 film stitched together in the horizontal (in-plane) direction and showing the segmented structure of the film. The leftmost part of the sequence is identical to Figure 4a$_1$. Magnified areas displayed below according to highlighted areas.

REFERENCES

1. Saelices, C. J.; Capron, I. Design of Pickering Micro- and Nanoemulsions Based on the Structural Characteristics of Nanocelluloses. *Biomacromolecules* **2018***, 19*, 460-469.

2. Fu, T.; Montes, F.; Suraneni, P.; Youngblood, J.; Weiss, J. The Influence of Cellulose Nanocrystals on the Hydration and Flexural Strength of Portland Cement Pastes. *Polymers* **2017***, 9*, 1-16.

3. Reid, M. S.; Villalobos, M.; Cranston, E. D. Benchmarking Cellulose Nanocrystals: From the Laboratory to Industrial Production. *Langmuir* **2017***, 33*, 1583-1598.

4. Du, L.; Zhong, T.; Wolcott, M. P.; Zhang, Y.; Qi, C.; Zhao, B.; Wang, J.; Yu, Z. Dispersing and stabilizing cellulose nanoparticles in acrylic resin dispersions with unreduced transparency and changed rheological property. *Cellulose* **2018***, 25*, 2435-2450.

5. Semenikhin, N. S.; Kadasala, N. R.; Moon, R. J.; Perry, J. W.; Sandhage, K. H. Individually Dispersed Gold Nanoshell-Bearing Cellulose Nanocrystals with Tailorable Plasmon Resonance. *Langmuir* **2018***, 34*, 4427-4436.

6. Zoppe, J. O.; Dupire, A. V. M.; Lachat, T. G. G.; Lemal, P.; Rodriguez-Lorenzo, L.; Petri-Fink, A.; Weder, C.; Klok, H. Cellulose Nanocrystals with Tethered Polymer Chains: Chemically Patchy versus Uniform Decoration. *ACS Macro Letters* **2017***, 6*, 892-897.